



# An Organic Redox Flow Cell-Inspired Paper-Based Primary Battery

Marina Navarro-Segarra<sup>+, [a]</sup>, Perla Patricia Alday<sup>+, [a]</sup>, David Garcia,<sup>[a]</sup> Omar A. Ibrahim,<sup>[b]</sup> Erik Kjeang,<sup>[b]</sup> Neus Sabaté,<sup>[a, c]</sup> and Juan Pablo Esquivel<sup>\*[a]</sup>

A portable paper-based organic redox flow primary battery using sustainable quinone chemistry is presented. The compact prototype relies on the capillary forces of the paper matrix to develop a quasi-steady flow of the reactants through a pair of porous carbon electrodes without the need of external pumps. Co-laminar capillary flow allows operation Under mixed-media conditions, in which an alkaline anolyte and an acidic catholyte are employed. This feature enables higher electrochemical cell voltages during discharge operation and the utilization of a wider range of available species and elec-

trolytes and provides the advantage to form a neutral or near-neutral pH as the electrolytes neutralize at the absorbent pad, which allows a safe disposal after use. The effects of the device design parameters have been studied to enhance battery features such as power output, operational time, and fuel utilization. The device achieves a faradaic efficiency of up to 98%, which is the highest reported in a capillary-based electrochemical power source, as well as a cell capacity of up to  $11.4 \text{ Ah L}^{-1} \text{ cm}^{-2}$ , comparable to state-of-the-art large-scale redox flow cells.

## Introduction

The increasing usage of small-sized portable electronic devices in recent decades has led to a strong demand for miniaturized power sources. Moreover, such devices require batteries to be adapted to product sizes and form factors that make their recycling even more challenging, since it is much harder to separate the battery from the device, thus aggravating the environmental impact associated to the generation of waste electrical and electronic equipment (WEEE). WEEE is rapidly becoming the largest waste stream worldwide.<sup>[1,2]</sup> According to a report from the World Economic Forum, the material value of our spent electronic devices globally amounts to \$62.5 billion, which is three times more than the annual output of the world's silver mines.<sup>[3]</sup> Indeed, WEEE can be a source of highly valuable materials but still it will require energy and resources to manage, collect, process, and repurpose. WEEE should be

properly managed but nowadays is sent away to places in the world where it can cause environmental and health problems.<sup>[4]</sup> The problem is even more critical when this waste is not even collected properly and ends up in landfills where, in many cases, it is incinerated. One of the most hazardous components in e-waste is batteries, as they need special and dedicated recycling processes.<sup>[5]</sup> To date, the portable energy demand has been mostly fulfilled with inexpensive primary alkaline and button cell batteries. Unfortunately, these power sources are disposed of after use, sometimes even before being completely depleted, causing significant energy waste and environmental damage if not properly collected and recycled.<sup>[6-9]</sup> This is reflected in the percentage of primary batteries that are collected for recycling in Europe: in 2017, approximately 226 000 tons of portable batteries and accumulators were sold in the EU-28, whereas only about 100 000 tons of waste portable batteries and accumulators were collected for recycling, representing approximately 45%.<sup>[10]</sup> For this reason, other alternatives for sustainable energy storage are being developed, such as redox flow batteries, fuel cells, and, more recently, microfluidic fuel cells.<sup>[11-13]</sup> These devices rely on the use of liquid fuels that are either oxidized or reduced at the device electrodes. Very often, these power sources make use of oxygen reduction as cathodic species, which allows them to become lighter and more efficient.



Concerning fuel choices, many chemistries have been tested with promising results; for example, methanol, ethanol, hydrogen or formic acid have been widely explored, owing to their promising theoretical specific energies. However, although these fuels are seen as benign, their operation often requires precious metals (e.g., Pt, Pd, Ru) as catalysts, which excludes them as primary battery replacements. In this sense, new ap-


[a] M. Navarro-Segarra,<sup>+</sup> Dr. P. P. Alday,<sup>+</sup> D. Garcia, Prof. N. Sabaté, Dr. J. P. Esquivel  
Instituto de Microelectrónica de Barcelona, IMB-CNM (CSIC)  
C/ dels Til·lers sn, Campus UAB, 08193 Bellaterra, Barcelona (Spain)  
E-mail: [juanpablo.esquivel@csic.es](mailto:juanpablo.esquivel@csic.es)

[b] Dr. O. A. Ibrahim, Prof. E. Kjeang  
Fuel Cell Research Lab (FCReL), School of Mechatronic Systems Engineering  
Simon Fraser University, V3T 0A3 Surrey, BC (Canada)

[c] Prof. N. Sabaté  
Catalan Institution for Research and Advanced Studies (ICREA)  
Passeig Lluís Companys 23, 08010 Barcelona (Spain)

[†] These authors contributed equally to this work.

 Supporting Information and the ORCID identification number(s) for the author(s) of this article can be found under:  
 <https://doi.org/10.1002/cssc.201903511>.

 This publication is part of a Special Issue focusing on "Organic Batteries". Please visit the issue at <http://doi.org/10.1002/cssc.v13.9>.

proaches have been reported, in which catalyst-free redox chemistries, such as all-vanadium, zinc/bromide, or polysulfide/bromide, are used as fuel in fluidic systems that only require inexpensive carbon material electrodes to collect the current.<sup>[14]</sup> However, these inorganic compounds involve toxic and environmentally nonfriendly elements. For this reason, organic active species have arisen as a more sustainable alternative. In particular, quinones are organic compounds that have been recently identified as suitable candidates because they are sustainable, benign, abundant, and inexpensive.<sup>[15,16]</sup> The developed quinone-based redox batteries have already demonstrated their viability for large-scale energy storage applications.<sup>[17–19]</sup> Portable approaches for these organic redox flow batteries were reported by Yang et al. in 2014 and Ibrahim et al. in 2017, both of which used water-based solutions of an anthraquinone as the negative electrode and benzoquinone as the positive one, yielding power densities of around  $4 \text{ mW cm}^{-2}$  with 0.6 V open circuit potential.<sup>[20,21]</sup> Despite good performance, the vast majority of flow cells require external pumps to maintain the flow of reactants. This fact increases the device complexity and reduces its integration capacity and overall energy efficiency.<sup>[22,23]</sup> A smart way of overcoming this drawback has been assessed for micro-scale fuel cells with capillary-based microfluidics, which rely on paper and other porous matrices for fluid transport and thus eliminate the need for external pumps.<sup>[24–28]</sup> Paper-based microfluidic fuel cells have already demonstrated their feasibility with well-known fuels, such as methanol, ethanol, hydrogen, or formic acid.<sup>[29–33]</sup> However, as mentioned above, the need for noble metal catalysts prevents their usability as primary power sources. Other paper-based approaches have used glucose as fuel, which can be scavenged with enzymatic catalysts.<sup>[34–36]</sup> Nevertheless, their implementation in real environments is still challenging, as biocatalysts have restricted stability, lack reproducibility, and yield very low power outputs. A first validation of a redox battery using quinone species in a paper matrix was reported in 2017 by Esquivel et al.,<sup>[37]</sup> who showed portable power generation and a biotic degradation of the whole device. The reported approach can potentially eliminate end-of-life concerns posed by current primary battery technologies, as the devices are conceived to be discarded after use without the need for any specific recycling facilities because of their all-organic nature, causing no harm to the environment where they are disposed of. The prototype, although promising, yielded faradaic efficiencies below 3%, owing to its diffusion-driven operation.

The work presented herein proposes the use of sustainable benign organic chemistries to generate energy in a portable paper-based flow battery. This organic redox battery relies on capillary forces to flow the reactants. Its versatile design allows almost complete fuel utilization with a high cell capacity. In this way, the fuel volume and weight can be highly optimized, which is a critical requirement for any feasible application of a power source for portable devices.

## Results and Discussion

### Device design and operation principle

The device presented herein is a compact and lightweight paper-based primary battery inspired in the working operation of a redox flow cell. Figure 1 shows a picture of a ready-to-use prototype. The device main structure consists of two parallel

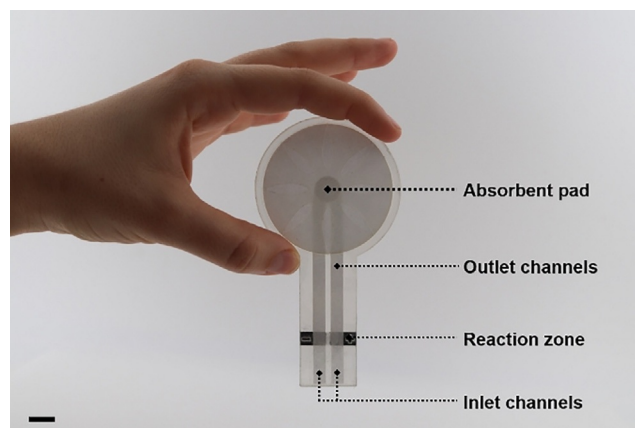


Figure 1. Paper-based capillary flow redox primary battery. Scale bar = 1 cm.

paper strips connected to a circular paper pad. The prototype is designed to start operating by immersing one of its ends in a reservoir that contains two small chambers with different solutions of electroactive species. The paper strip ends absorb the fluids contained in the chambers establishing a convective flow of reactants by capillary force. A carbon electrode placed on each of the paper channels allows the redox species to react (i.e., oxidize and reduce) and thus enable energy generation. A small segment of paper connects both channels, acting as a salt bridge between the electrodes. The device keeps functioning until the round pad at the end is completely filled up. Depending on the size, material, and design of the absorbent pad, the operating time of the battery can expand from a few minutes to half an hour. Moreover, the battery can easily be recharged by replacing the wet absorbent pad with a dry component and refilling the fuel reservoir with additional electroactive species. The capillary-based paper battery has been designed as a hand-sized device. A  $20 \times 5 \text{ mm}$  piece of paper, forming a U shape, provides the inlet channels to the solutions and at the same time, constitutes the battery salt bridge. Two outlet channels of  $55 \times 5 \text{ mm}$  connected with the electrode region drive out the reaction products up to two stacked circular paper absorbent pads (10 and 50 mm diameter). The absorbent pad  $360^\circ$  shape is based on a quasi-steady flow strategy reported by Adkins et al., where a  $270^\circ$  fan-shaped absorbent was used to create a steady capillary flow for the first time.<sup>[38]</sup> The paper assembly is fed with quinone redox species solutions already dissolved in a  $25 \times 15 \times 5 \text{ mm}$  poly(methyl methacrylate) reservoir.

As in membrane-less microfluidic co-laminar flow cells, this capillary flow cell facilitates operation under mixed-media conditions, in which an alkaline negative electrode and an acidic positive electrode are employed. This feature enables higher electrochemical cell voltages during discharge operation and the utilization of a wider range of available species and electrolytes.<sup>[21]</sup> Additionally, mixed-media operation provides the advantage of a neutral or near neutral pH as the acidic and alkaline neutralize at the absorbent pad, which allows a safe disposal after operation. Therefore, the flow battery was characterized with a solution of 0.1 M *para*-benzoquinone (*p*-BQ) in 0.5 M oxalic acid as catholyte and a solution of 0.1 M hydroquinone sulfonic acid potassium salt (H<sub>2</sub>BQS) in 1 M KOH as anolyte (see the Supporting Information, Figure S1). Quinone species concentrations were set to reach the *p*-BQ solubility limit in water.

The battery performance was tested by using an initial prototype configuration, where the carbon electrodes (5 mm length and 10 mm wide) were placed on the paper channels, providing the battery with a 0.25 cm<sup>2</sup> active area (Figure 2a and Figure S2). Once the performance of the initial battery design was validated, modifications of different design parameters of the cell were performed with the aim of improving the generated power output and redox species harnessing (i.e., faradaic efficiency). The design modifications and their effect on the battery output are presented in the following sections.

### Battery power output optimization

The initial design of battery prototype with 2D carbon electrodes was tested by immersing its inlet pads into the quinone solutions of the fuel reservoirs. A stable value of  $0.75 \pm 0.05$  V was obtained, showing good correlation with the OCV values reported in prior studies of quinone chemistry.<sup>[21,37]</sup> Figure 2c shows the polarization and power density curves obtained during battery operation. The maximum power density was recorded to be 0.02 mW. After that, the device was connected to a 1.6 k $\Omega$  load to characterize the battery's continuous operation. Figure S3 shows the voltage and current output. A quasi-stable power output value was achieved for approximately 6 minutes (Figure 2d). After this time, the absorbent pad was completely filled up and the capillary flow regime stopped. Consequently, the battery power output diminishes significantly due to the lack of convective flow. To enhance the battery power output, the available electroactive area of the carbon electrodes was increased by applying a thermal treatment that improved their hydrophilicity. The electrode's hydrophilicity allows the liquid to flow through the porous carbon microstructure, turning a 2D electroactive area (flow-over electrode) into a 3D one (flow-through electrode) while keeping the overall device dimensions (Figure 2b). The battery electrochemical performance of the 3D electrode configurations is shown in Figures 2c. The performance when subjected to a fixed ohmic load of 230  $\Omega$  is shown in Figure 2d and Figure S3.

Allowing the reactant species to flow through the 3D electrodes leads to a 20-fold improvement in the power peak delivered by the cell, that is, from a maximum value of 0.02 mW to 0.48 mW. The battery power output stability in time demonstrates that, despite using hydrophilic flow-through porous carbon electrodes, capillary flow established in the paper structure is kept steady without the need of external pumps. Thus the capillary pressure is not being altered by this modification and the battery power output is still stable.

The results obtained from the characterization of the battery under continuous operation until the saturation of the absorbent pad allow assessing its efficiency at both electrode configurations.<sup>[39]</sup> The faradaic efficiency ( $\eta_F$ ) allows evaluation of the electroactive species utilization, quantifying the theoretical charge capacity that is actually being converted into current, and is calculated by using Equation (1):

$$\eta_F = \frac{\int_0^t I(t) dt}{n c_0 V F} \quad (1)$$

where  $t$  is the measurement time,  $I(t)$  is the current extracted from the measured voltage divided by the resistance of the fixed load,  $n$  is the number of electrons per mole,  $F$  is the Faraday constant,  $c_0$  is the initial species concentration, and  $V$  is the volume of diluted redox species. Moreover, the energy efficiency ( $\eta_E$ ) of the capillary flow cell can be evaluated by

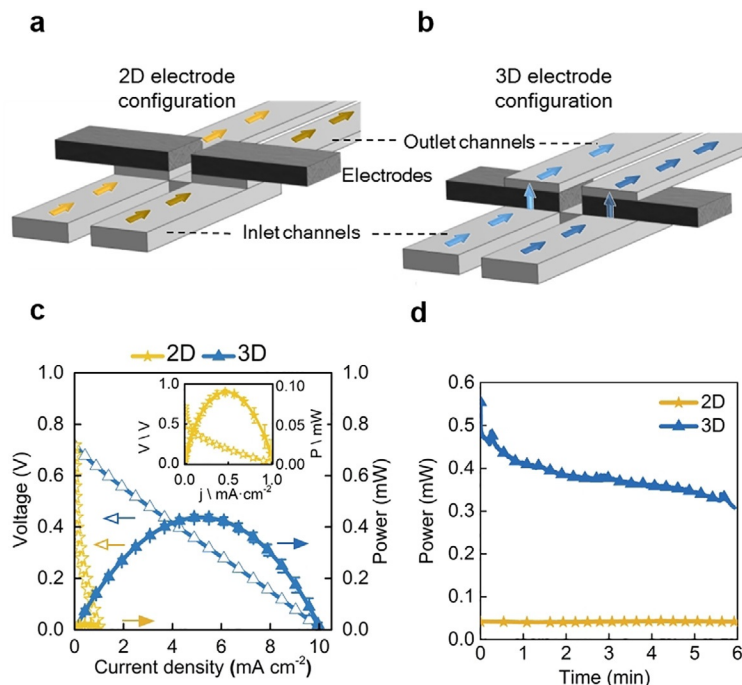


**Figure 2.** a) Flow-over electrode configuration. b) Flow-through electrode configuration. c) Polarization curves of the capillary flow battery designs with flow-over and flow-through electrode configurations. d) Discharge curves of the capillary paper-based battery when subjected to fixed external loads that correspond to the operating point of maximum power in flow-through (230  $\Omega$ ) and flow-over (1600  $\Omega$ ) configurations. Data points and lines represent mean values for  $n = 3$ .

comparing the power delivered by the device under continuous operation to the energy that the battery cell could deliver ideally, that is, when working at its theoretical voltage [Equation (2)]:

$$\eta_E = \frac{\int_0^t I(t) \cdot E(t) dt}{n C_0 V F E} \quad (2)$$

where  $E(t)$  is the operating voltage and  $E$  is the theoretical Nernst voltage of the cell. The faradaic and energy efficiencies obtained from the continuous operation curves of the 2D and 3D battery cells show that the 3D configuration allows a significant improvement in the species conversion when compared to the 2D, as the faradaic efficiency increases from 2.3% to 21%. Likewise, the improvement of both power output and species harnessing translates into a higher energy efficiency of the battery with 3D electrode configuration as it increases from 0.7% to 6.8%.

### Capillary flow rate modification and influence on fuel utilization

One way of increasing the percentage utilization of redox species is to increase their residence time at the electrodes. As reactants are pumped by capillary force, the liquid flow rate was modified by changing the overall fluidic resistance of the battery paper structure. In particular, lower flow velocities were achieved by increasing the output channel length ( $L_C$ ) from 20 mm to 40 mm and 60 mm (see below, Figure 4a). The generated capillary flow rates were characterized by measuring the evolution of the liquid front in the absorbent pad. Figure 3a shows the total wetted area of the absorbent pad at different times or the three different channel lengths. The linear relationship between the absorbed liquid volume in the circular pad with time allows the flow rate of reactants to be derived. Knowing the absorbent volumetric capacity,  $C$ , of the paper pad ( $7 \mu\text{L mm}^{-2}$ ), the flow rate  $Q$  ( $\mu\text{L cm}^{-2}$ ) can be calculated by using Equation (3),

$$Q = \frac{\Delta A}{\Delta t} \cdot C \quad (3)$$

where  $\Delta A$  is the cross-sectional vector area increment ( $\text{cm}^2$ ) and  $\Delta t$  is the time increment. Figure 3b shows the obtained

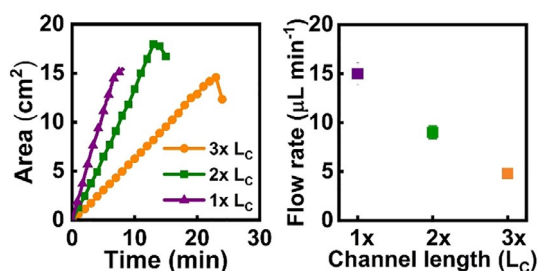


**Figure 3.** a) Liquid-covered absorbent pad area evolution over time. b) Resulting capillary flow rates for different output channel lengths ( $L_C$ ). Data points represent mean values for  $n = 3$ .

flow rate values; as expected, the magnitude of the flow rate decreases on increasing the output channel length. Moreover, as the total capacity of the absorbent pad is fixed, the operating time of the device is inversely proportional to the established flow rate. As a result, the operational time of the battery expanded up to 25 minutes when the flow rate was diminished to  $4.8 \mu\text{L min}^{-1}$ .

The electrochemical performance of the flow-through cell was tested under different flow rates. Again, in all cases the devices reached a stable OCV value of  $0.75 \pm 0.05$  V. Figure 4b shows the maximum power values recorded at the  $I$ - $V$  curves for each flow rate, yielding  $0.48 \pm 0.01$  mW at  $15 \mu\text{L min}^{-1}$ ,  $0.47 \pm 0.02$  mW at  $9 \mu\text{L min}^{-1}$  and  $0.44 \pm 0.01$  mW at  $4.8 \mu\text{L min}^{-1}$ . Then, the batteries were operated under a fixed external ohmic load and their discharge curve was recorded. The mean power delivered by each cell is also shown in Figure 4b. The values of the energy and faradaic efficiencies obtained from the discharge curves are shown in Figure 4c.

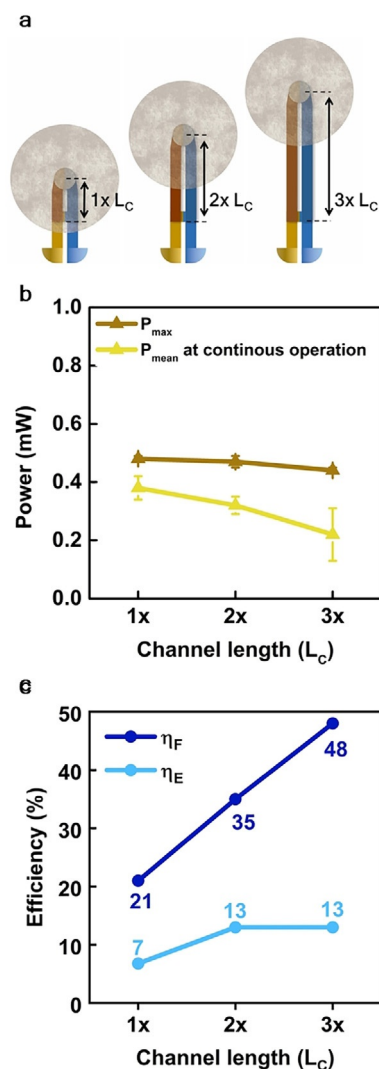


**Figure 4.** a) Maximum and mean powers of capillary flow battery at different reactant flow rates. b) Maximum and mean power and c) faradaic and energy efficiencies for each capillary flow battery tested channel length. Data points represent mean values for  $n = 3$ .

Lower flow rates yield better faradaic efficiencies, achieving a maximum of 48% of fuel conversion at  $4.8 \mu\text{Lmin}^{-1}$ . However, there is a trade-off between generated power and faradaic efficiency, as, although lower flow rates lead to increased operational times and electroactive species conversion rates, they deliver lower power outputs, owing to reduced electrode mass transport. Regarding energy efficiency, these two opposite effects compensate, yielding energy efficiencies of around 10% in all tested cases.

### Influence of electrode length on fuel utilization

With the aim of further improving the power output of the device, we decided to increase the electrode reaction zone of the battery. Therefore, the length of the porous carbon electrodes ( $L_E$ ) was increased sequentially from 5 mm (1x) to 10 mm (2x), 15 mm (3x), and 20 mm (4x). Figure 5a shows a comparison of the different tested geometries. The  $I$ - $V$  curves were measured and the maximum power obtained for each of the

geometric designs is depicted in Figure 5b. It can be seen that power generated by the flow battery increases with the increase of the electrode reaction area, although the most relevant change takes place between the 1x to 2x configurations. At increasing electrode lengths, the improvement was smaller, reaching a maximum power of 0.71 mW for an electrode length of 20 mm (4x configuration). The flow batteries were also subjected to continuous operation with a fixed external ohmic load. The mean power values of the discharge curves are given in Figure 5b. As expected, the average power output of the battery increases with electrode size and recovers the 0.44 mW obtained previously at higher flow rates. Finally, the fuel utilization efficiency was calculated. Figure 5c shows a significant increase in efficiency at growing electrode sizes, achieving an outstanding 98% value for the  $4 \times L_E$  configuration, meaning that practically all the electroactive species flown through the paper cell are converted to electrical power.

The power densities obtained with our capillary-based redox flow battery, with a maximum value of  $1.92 \text{ mWcm}^{-2}$ , yield within the same range of power previously reported for all-quinone and externally pumped flow batteries by Yang et al. and Ibrahim et al.<sup>[20,21]</sup> Moreover, this value is in good agreement with a previously reported value of  $1.8 \text{ mWcm}^{-2}$  by Esquivel et al. for a paper-based system.<sup>[37]</sup> This demonstrates the feasibility of using capillarity as sole pumping force while keeping power generation capability. In addition, it has been proven that device design can be adjusted to tune its flow rate, power density, operational time and faradaic efficiency. In particular, the circular geometry of the absorbent pad allows establishing a quasi-steady flow regime that provides stability to the cell electrochemical response. In this way, the paper-based flow system can benefit from the performance versatility that before was only available for flow cells provided with external pumps and can adapt to any specific application requirement.

In addition, flow rate and electrode design optimization allows the highest faradaic efficiency reported to date for paper-based microfluidic electrochemical power sources. Figure 6 depicts a comparison of faradaic and energy efficiencies of several reported devices. Most of the systems yield faradaic efficiencies of 1–10%. Some remarkable values of 30–40% were achieved with devices reported by Pasala et al. and Gonzala-

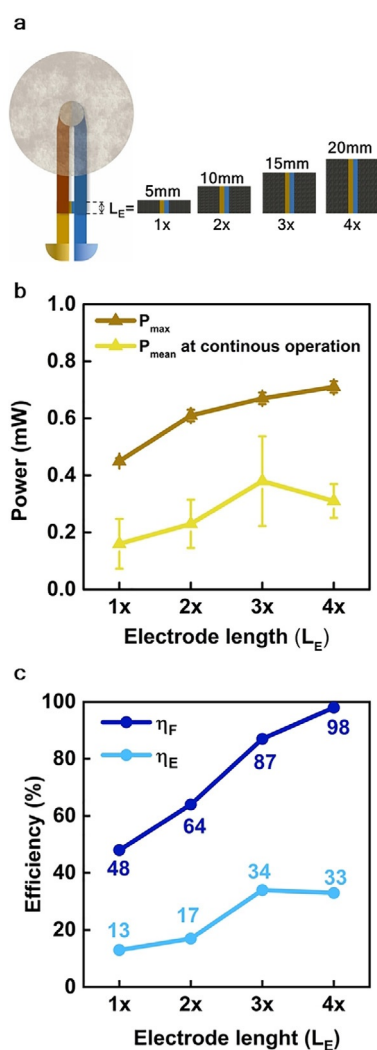


**Figure 5.** a) Electrode length ( $L_E$ ) modification scheme. b) Maximum and mean power and c) efficiencies yielded by the flow batteries with four electrode lengths. Data points mean values for  $n = 3$ .

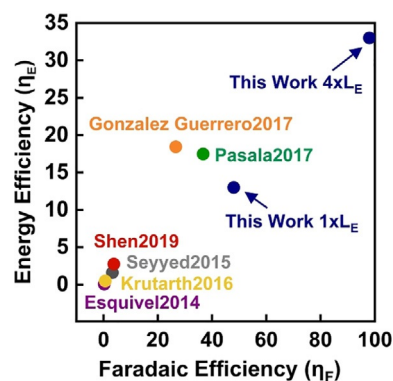


**Figure 6.** Comparison of faradaic and energy efficiencies of reported microfluidic paper-based fuel cells.

lez-Guerrero et al. in 2017.<sup>[28,34]</sup> Our optimized flow cell reaches a conversion rate of 48% and 98% (with 1× and 4× electrode lengths, respectively), which also impacts the energy efficiency, archiving a noteworthy 13% and 34% (with the same two electrode lengths).

The performance of the paper flow cell presented herein has been also compared to pump-assisted aqueous flow batteries with more traditional formats. Figure 7 shows a comparison in terms of cell capacity and cell energy density. These figures of

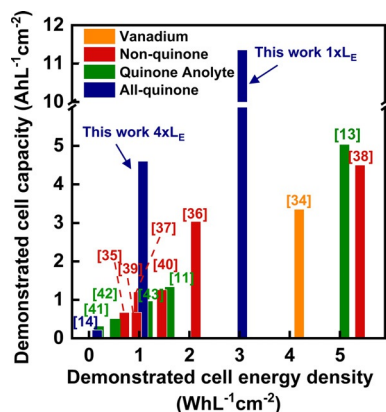


**Figure 7.** Comparison of demonstrated cell capacity and cell energy density of reported pump-assisted aqueous flow batteries.

merit were calculated as reported by Jin et al.,<sup>[19]</sup> that is, cell capacity was calculated by  $(C_{\text{CLS}}/V_{\text{tot}}) \times \Phi$ , where  $C_{\text{CLS}}$  is the capacity of the capacity limit side of the cell,  $V_{\text{tot}}$  is the volume of both redox solutions, and  $\Phi$  is the percentage of utilized capacity; cell energy density was obtained multiplying cell capacity by the open-circuit voltage at 50% state of charge. The values obtained were then normalized by the projected area of each of the reported cells, to end up in normalized units considering volumetric and areal features. Reactant volumes and electrode areas were extracted from each of the articles. The depicted values have been classified depending on the chemistry used in the devices, that is, a vanadium chemistry representative battery;<sup>[40]</sup> non-quinone batteries, comprising different chemistries, from viologen derivatives anolyte batteries coupled with ferrocene derivatives,<sup>[41,42]</sup> ammonium ferrocyanide ( $\text{NH}_3[\text{Fe}(\text{CN})_6]$ )<sup>[43]</sup> or TEMPO derivatives,<sup>[44]</sup> to a phenazine-based<sup>[45]</sup> or alloxazine-based<sup>[46]</sup> anolyte coupled with a  $\text{K}_3[\text{Fe}(\text{CN})_6]$  catholyte; quinone anolyte-based flow batteries coupled with potassium ferricyanide as cathode species,<sup>[17,19,47–49]</sup> and a fully quinone based battery.<sup>[20]</sup>

The high efficiency achieved by our cell is transferred into outstanding cell capacities of 11.4 and 4.6  $\text{Ah L}^{-1} \text{cm}^{-2}$ , with 1× and 4× electrode length, respectively. With respect to cell energy density, redox chemistries based on vanadium or viologen derivatives achieved higher values than the fully quinone-based chemistries. In this sense, our cell outperforms the cell presented by Yang et al., which also reported an all-quinone battery.<sup>[50]</sup> In their case, using a benzoquinone cathode and an anthraquinone anode, a 0.16  $\text{Wh L}^{-1} \text{cm}^{-2}$  cell energy density

was achieved, which is significantly lower than the 1.1 and 3.1  $\text{Wh L}^{-1} \text{cm}^{-2}$  achieved by our cell with 1× and 4× electrode lengths. Moreover, our cell approach does not need any ancillary device to flow the reactants, so the energy density provided can be considered as a net energy value.

## Conclusions

The paper-based primary battery presented herein departs from the operating principle of an organic redox flow cell but makes use of only the first discharge cycle. The new cell design allowed the establishment of a steady capillary-based flow rate that led to stable battery performance under mixed-media conditions. These features allowed direct use of available quinones by using an alkaline negative half-cell and an acidic positive half-cell with the added benefit of downstream neutralization for safe disposal. This work provides comprehensive guidelines and design rules to define how certain parameters, such as channel and electrode lengths, allow adjustment of the flow rates, power densities and fuel utilization in paper-based microfluidic devices. The current device design provides energy autonomy for about half an hour, which is sufficient for powering numerous single-use applications, such as portable diagnostics. However, its versatile design allows the operational time to be scaled by replacing the absorbent pad with one of higher liquid capacity and refilling the reservoir if necessary. In this sense, the paper flow cell acts as an energy converter in the same way as in traditional flow batteries, in which energy and power can be decoupled and adjusted to the application. In the current case, energy is related to the capacity of absorbent pad and species reservoir, whereas power relies on capillary flow rate and electrode area. The proof-of-concept device demonstrated its operation with an all-organic redox couple with a high fuel utilization and cell capacity and could be tested with further chemistries that led to energy capacities competitive with commercial portable primary batteries. Furthermore, strategies to promote liquid evaporation from the absorbent pad can expand operational times of the system up to days or even weeks, which would open new fields of applications of these novel eco-friendly power sources in sectors like the Internet of Things, precision agriculture, or environmental monitoring.

## Experimental Section

### Chemicals

Commercially available quinone redox species, *p*-Benzoquinone (*p*-BQ) and hydroquinone sulfonic acid potassium salt ( $\text{H}_2\text{BQS}$ ), and electrolytes, oxalic acid, and potassium hydroxide were purchased from Sigma–Aldrich (Sigma Aldrich, St Louis, Missouri, USA) and used as received, as well as the colorants used for the flow rate characterization, euroglaucline disodium salt and tartrazine dyes. All solutions were prepared in deionized water; 0.1 M *p*-BQ in 0.5 M oxalic acid and 0.1 M  $\text{H}_2\text{BQS}$  in 1 M KOH were used as catholyte and anolyte, respectively.

## Device fabrication

Glass fiber (Standard 17, 340  $\mu\text{m}$ ) strips are used as inlet channels whereas cellulose (Whatman1; 180  $\mu\text{m}$ ) is used as outlet paper channels and absorbent pad. Both materials from GE Healthcare, Pittsburgh, PA, USA. The device structure was assembled using pressure sensitive adhesives (PSA) (Adhesives Research, Glen Rock, PA, USA). A custom-made support was fabricated in 6 mm thick poly(methyl methacrylate) (Plexiglas, Evonik Performance Materials GmbH, Darmstadt, Germany) to characterize the device. The device components were designed in a CAD program (CorelDRAW, Corel, Ottawa, ON, Canada). All components were cut by using a CO<sub>2</sub> laser cutter (Mini 24, Epilog Laser, Golden, CO, USA) and manually assembled layer by layer by using templates and alignment pins. Porous carbon electrodes were cut to size from sheets of Toray carbon paper (TGPH-120; E-TEK) with thickness of 370  $\mu\text{m}$ . For the purpose of this work, the porous carbon electrodes were annealed in a butane flame to confer the hydrophilic behavior needed for the flow-through configuration.<sup>[51]</sup> To carry out the experiments, the device was placed on a custom-made acrylic support that comprised two solution wells where the species were dissolved in their respective electrolytes, facilitated electrical connection to the electrodes and include a reusable lid to prevent evaporation while allowing purging of air as the absorbent pad is filled.

## Flow characterization

The evolution of the capillary flow rate along the paper channels over time was characterized by measuring the progress of the liquid front in the absorbent pad. To enhance image contrast, in these experiments, 100 mM solutions of euroglaucline disodium salt and tartrazine dyes were used to simulate and visualize anolyte and catholyte flow. The images were recorded with a web camera (C920, Logitech, Fremont, CA, USA) controlled by time-lapse software (VideoVelocity, CandyLabs, Vancouver, BC, Canada), which saved images at a rate of 1 frame every 5 s. The flow rates were calculated from the captured images by measuring the increase in the absorbent pad area covered by the dyed solutions over time. The images were analyzed by using ImageJ software (US National Institutes of Health, Bethesda, Maryland, USA).

## Battery electrochemical characterization

The open-circuit voltage ( $V_{\text{oc}}$ ) of each cell was measured before polarization. Polarization curves were performed at room temperature in potentiodynamic mode at a scan rate of 50 mV s<sup>-1</sup>. Chronopotentiometric curves were measured by using external loads selected for each kind of electrode configuration. All electrochemical characterization curves were recorded with a Dropsens  $\mu\text{Stat}$  400 potentiostat (Dropsens, Oviedo, Spain). Measurements were performed in triplicate for each cell at room temperature.

## Acknowledgements

The funding for this research provided through the Science for Solving Society's Problems Challenge by the Electrochemical Society and the Bill & Melinda Gates Foundation is highly appreciated. P.A. acknowledges support from CONACyT through a scholarship to pursue postgraduate studies. N.S. is thankful for financial support received from ERC Consolidator Grant (SUPERCELL—GA.648518). Additional support from the Natural Sciences and

Engineering Research Council of Canada (NSERC), Canada Foundation for Innovation (CFI) and British Columbia Knowledge Development Fund (BCKDF) is also acknowledged. E.K. acknowledges support from the Canada Research Chairs program.

## Conflict of interest

The authors declare no conflict of interest.

**Keywords:** energy storage • microfluidics • organic batteries • quinones • redox flow batteries

- [1] R. Widmer, H. Oswald-Krapf, D. Sinha-Khetriwal, M. Schnellmann, H. Böni, *Environ. Impact Assess. Rev.* **2005**, *25*, 436–458.
- [2] V. Pérez-Belis, M. D. Bovea, V. Ibáñez-Forés, *Waste Manage. Res.* **2015**, *33*, 3–29.
- [3] "The world's e-waste is a huge problem. It's also a golden opportunity | World Economic Forum," can be found at <https://www.weforum.org/agenda/2019/01/how-a-circular-approach-can-turn-e-waste-into-a-golden-opportunity/>, accessed February 12, 2020.
- [4] "Electronic waste", World Health Organization, can be found at <https://www.who.int/ceh/risks/ewaste/en/>, accessed February 12, 2020.
- [5] "A New Circular Vision for Electronics, Time for a Global Reboot | World Economic Forum," can be found at <https://www.weforum.org/reports/a-new-circular-vision-for-electronics-time-for-a-global-reboot>, accessed February 12, 2020.
- [6] P. Kiddee, R. Naidu, M. H. Wong, *Waste Manage.* **2013**, *33*, 1237–1250.
- [7] L. Järup, *Br. Med. Bull.* **2003**, *68*, 167–182.
- [8] L. Moreno-Merino, M. E. Jiménez-Hernández, A. de la Losa, V. Huerta-Muñoz, *Sci. Total Environ.* **2015**, *526*, 187–195.
- [9] D. Larcher, J. M. Tarascon, *Nat. Chem.* **2015**, *7*, 19–29.
- [10] "Waste statistics: recycling of batteries and accumulators—Statistics Explained," can be found at [https://ec.europa.eu/eurostat/statistics-explained/index.php?title=Waste\\_statistics\\_-\\_recycling\\_of\\_batteries\\_and\\_accumulators](https://ec.europa.eu/eurostat/statistics-explained/index.php?title=Waste_statistics_-_recycling_of_batteries_and_accumulators), accessed February 12, 2020.
- [11] C. Ponce de León, A. Frías-Ferrer, J. González-García, D. A. Szánto, F. C. Walsh, *J. Power Sources* **2006**, *160*, 716–732.
- [12] E. Kjeang, N. Djilali, D. Sinton, *J. Power Sources* **2009**, *186*, 353–369.
- [13] J. Yang, S. Ghobadian, P. J. Goodrich, R. Montazami, N. Hashemi, *Phys. Chem. Chem. Phys.* **2013**, *15*, 14147–14161.
- [14] M. H. Chakrabarti, N. P. Brandon, S. A. Hajimolana, F. Tariq, V. Yufit, M. A. Hashim, M. A. Hussain, C. T. J. Low, P. V. Aravind, *J. Power Sources* **2014**, *253*, 150–166.
- [15] C. Han, H. Li, R. Shi, T. Zhang, J. Tong, J. Li, B. Li, *J. Mater. Chem. A* **2019**, *7*, 23378–23415.
- [16] J. Winsberg, T. Hagemann, T. Janoschka, M. D. Hager, U. S. Schubert, *Angew. Chem. Int. Ed.* **2017**, *56*, 686–711; *Angew. Chem.* **2017**, *129*, 702–729.
- [17] K. Lin, Q. Chen, M. R. Gerhardt, L. Tong, S. B. Kim, L. Eisenach, A. W. Valle, D. Hardee, R. G. Gordon, M. J. Aziz, M. P. Marshak, *Science* **2015**, *349*, 1529–1532.
- [18] X. Wei, W. Duan, J. Huang, L. Zhang, B. Li, D. Reed, W. Xu, V. Sprenkle, W. Wang, *ACS Energy Lett.* **2016**, *1*, 705–711.
- [19] S. Jin, Y. Jing, D. G. Kwabi, Y. Ji, L. Tong, D. De Porcellinis, M. A. Goulet, D. A. Pollack, R. G. Gordon, M. J. Aziz, *ACS Energy Lett.* **2019**, *4*, 1342–1348.
- [20] B. Yang, L. Hooper-Burkhardt, F. Wang, G. K. Surya Prakash, S. R. Narayanan, *J. Electrochem. Soc.* **2014**, *161*, A1371–A1380.
- [21] O. A. Ibrahim, P. Alday, N. Sabaté, J. P. Esquivel, E. Kjeang, *J. Electrochem. Soc.* **2017**, *164*, A2448–A2456.
- [22] E. Kjeang, B. T. Proctor, A. G. Brolo, D. A. Harrington, N. Djilali, D. Sinton, *Electrochim. Acta* **2007**, *52*, 4942–4946.
- [23] S. A. Mousavi Shaegh, N. T. Nguyen, S. H. Chan, *Int. J. Hydrogen Energy* **2011**, *36*, 5675–5694.
- [24] I. Jang, S. Song, *Lab Chip* **2015**, *15*, 3405–3412.
- [25] R. K. Arun, S. Halder, N. Chanda, S. Chakraborty, *Lab Chip* **2014**, *14*, 1661–4.

- [26] H. Liu, R. M. Crooks, *Anal. Chem.* **2012**, *84*, 2528–2532.
- [27] S. M. Mousavi Ehteshami, M. Asadnia, S. N. Tan, S. H. Chan, *J. Power Sources* **2016**, *301*, 392–395.
- [28] V. Pasala, K. Ramanujam, *Ionics* **2017**, *23*, 1811–1817.
- [29] C. A. López-Rico, J. Galindo-De-La-Rosa, E. Ortiz-Ortega, L. Álvarez-Contreras, J. Ledesma-García, M. Guerra-Balcázar, L. G. Arriaga, N. Arjona, *Electrochim. Acta* **2016**, *207*, 164–176.
- [30] J. P. Esquivel, F. J. Del Campo, J. L. Gómez De La Fuente, S. Rojas, N. Sabaté, *Energy Environ. Sci.* **2014**, *7*, 1744.
- [31] J. P. Esquivel, J. R. Buser, C. W. Lim, C. Domínguez, S. Rojas, P. Yager, N. Sabaté, *J. Power Sources* **2017**, *342*, 442–451.
- [32] K. H. Purohit, S. Emrani, S. Rodríguez, S. S. Liaw, L. Pham, V. Galvan, K. Domalaon, F. A. Gomez, J. L. Haan, *J. Power Sources* **2016**, *318*, 163–169.
- [33] L. L. Shen, G. R. Zhang, T. Venter, M. Biesalski, B. J. M. Etzold, *Electrochim. Acta* **2019**, *298*, 389–399.
- [34] M. J. González-guerrero, F. Javier, J. Pablo, D. Leech, *Biosens. Bioelectron.* **2017**, *90*, 475–480.
- [35] L. del Torno-de Román, M. Navarro, G. Hughes, J. P. Esquivel, R. D. Milton, S. D. Minter, N. Sabaté, *Electrochim. Acta* **2018**, *282*, 336–342.
- [36] Z. Zhu, T. Kin Tam, F. Sun, C. You, Y. H. Percival Zhang, *Nat. Commun.* **2014**, *5*, 3026.
- [37] J. P. Esquivel, P. Alday, O. A. Ibrahim, B. Fernández, E. Kjeang, N. Sabaté, *Adv. Energy Mater.* **2017**, *7*, 1700275.
- [38] J. A. Adkins, E. Noviana, C. S. Henry, *Anal. Chem.* **2016**, *88*, 10639–10647.
- [39] R. Jiang, C. Rong, D. Chu, *J. Power Sources* **2004**, *126*, 119–124.
- [40] L. Li, S. Kim, W. Wang, M. Vijayakumar, Z. Nie, B. Chen, J. Zhang, G. Xia, J. Hu, G. Graff, J. Liu, Z. Yang, *Adv. Energy Mater.* **2011**, *1*, 394–400.
- [41] B. Hu, C. DeBruler, Z. Rhodes, T. L. Liu, *J. Am. Chem. Soc.* **2017**, *139*, 1207–1214.
- [42] E. S. Beh, D. De Porcellinis, R. L. Gracia, K. T. Xia, R. G. Gordon, M. J. Aziz, *ACS Energy Lett.* **2017**, *2*, 639–644.
- [43] J. Luo, B. Hu, C. Debruler, Y. Bi, Y. Zhao, B. Yuan, M. Hu, W. Wu, T. L. Liu, *Joule* **2019**, *3*, 149–163.
- [44] T. Janoschka, N. Martin, M. D. Hager, U. S. Schubert, *Angew. Chem. Int. Ed.* **2016**, *55*, 14427–14430; *Angew. Chem.* **2016**, *128*, 14639–14643.
- [45] A. Hollas, X. Wei, V. Murugesan, Z. Nie, B. Li, D. Reed, J. Liu, V. Sprenkle, W. Wang, *Nat. Energy* **2018**, *3*, 508–514.
- [46] K. X. Lin, R. Gómez-Bombarelli, E. S. Beh, L. C. Tong, Q. Chen, A. Valle, A. Aspuru-Guzik, M. J. Aziz, R. G. Gordon, *Nat. Energy* **2016**, *1*, 16102.
- [47] Y. Ji, M. Goulet, D. A. Pollack, D. G. Kwabi, S. Jin, D. Porcellinis, E. F. Kerr, R. G. Gordon, M. J. Aziz, *Adv. Energy Mater.* **2019**, *9*, 1900039.
- [48] D. G. Kwabi, K. Lin, Y. Ji, E. F. Kerr, M.-A. Goulet, D. De Porcellinis, D. P. Tabor, D. A. Pollack, A. Aspuru-Guzik, R. G. Gordon, M. J. Aziz, *Joule* **2018**, *2*, 1894–1906.
- [49] Z. Yang, L. Tong, D. P. Tabor, E. S. Beh, M.-A. Goulet, D. De Porcellinis, A. Aspuru-Guzik, R. G. Gordon, M. J. Aziz, *Adv. Energy Mater.* **2018**, *8*, 1702056.
- [50] B. Yang, L. Hooper-Burkhardt, S. Krishnamoorthy, A. Murali, G. K. S. Prakash, S. R. Narayanan, *J. Electrochem. Soc.* **2016**, *163*, A1442–A1449.
- [51] E. Kjeang, R. Michel, D. A. Harrington, N. Djilali, D. Sinton, *J. Am. Chem. Soc.* **2008**, *130*, 4000–4006.

---

Manuscript received: December 22, 2019

Revised manuscript received: February 12, 2020

Accepted manuscript online: February 26, 2020

Version of record online: March 18, 2020